Synthetic Organic Design for Solar Fuel Systems

Julien Warnan*[a,b] and Erwin Reisner*[a]

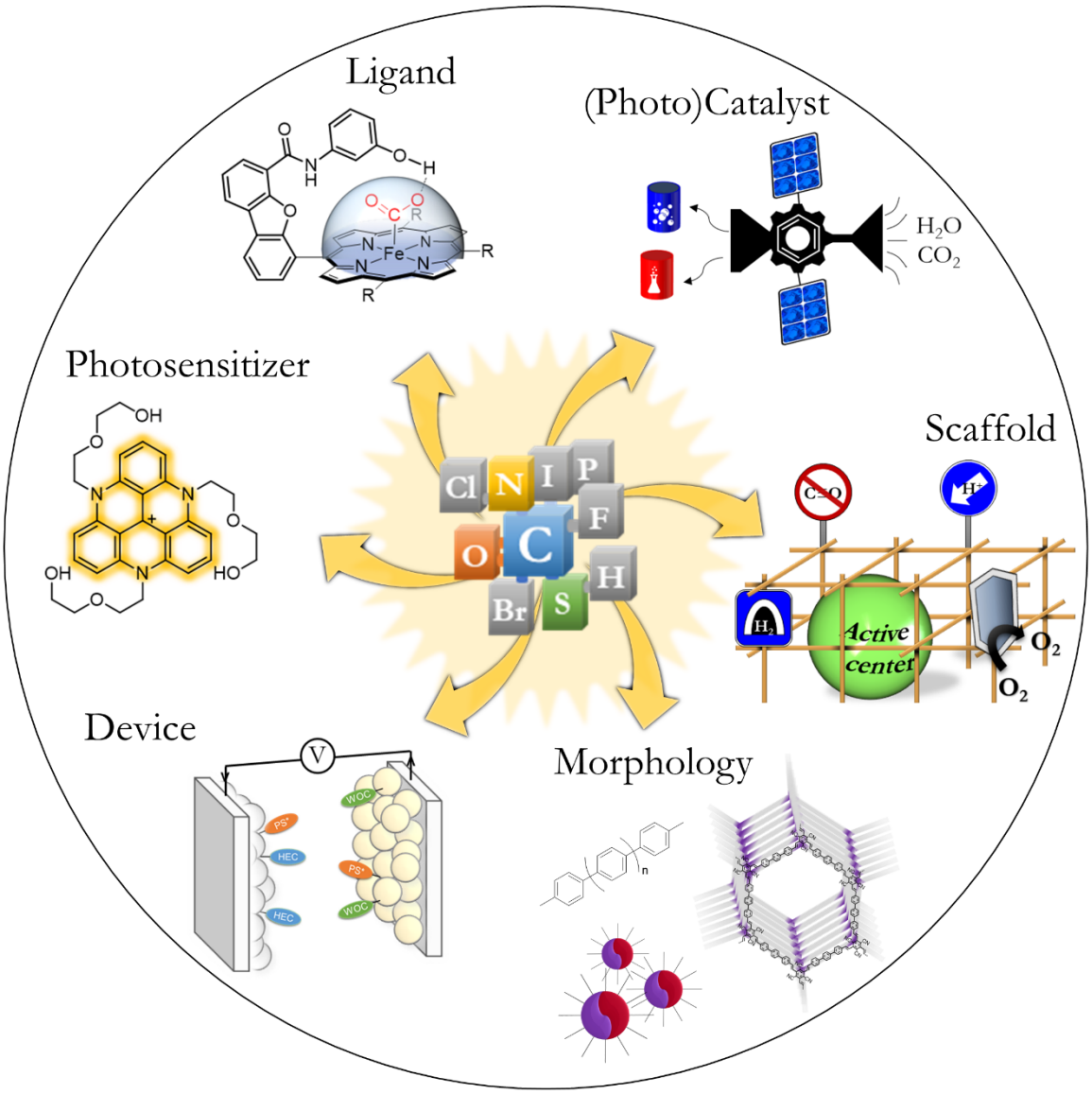

Abstract: From the understanding of biological processes and metalloenzymes to the development of inorganic catalysts, electro- and photocatalytic systems for fuel generation have evolved considerably during the last decades. Recently, organic and hybrid organic systems have emerged to challenge the classical inorganic structures through their enormous chemical diversity and modularity that led earlier to their success in organic (opto)electronics. This Minireview describes recent advances in the design of synthetic organic architectures and promising strategies toward (solar) fuel synthesis, highlighting progress on materials from organic ligands and chromophores to conjugated polymers and covalent organic frameworks.

1. Introduction

Since the demonstration of photoelectrochemical water splitting using the semiconductor (SC) TiO_2 and the H_2 evolution catalyst (HEC) platinum, inorganic materials have dominated the field in both number and efficiency.[1] They still undergo fast development, but often lack understanding at an atomic level, which limits the flexibility and fine-tuning capabilities needed to rationally improve (photo)catalytic performance.

Biology, through photosynthesis and fuel-making enzymes even in non-photosynthetic organisms, provides blueprints for the design of dyes and catalysts with outstanding performance such as the light-harvesting complexes, H_2-evolving hydrogenase (H_2ase) and the CO_2 reductases.[2] The activity of these biocatalysts relies on the choreography of evolutionarily-developed design principles, including: active sites with an optimized primary and outer coordination sphere to stabilize reaction intermediates, efficient energy and electron transfers (ETs), well-aligned electroactive ligands and electron relays, as well as substrate and product channels.

Although some of these concepts are being implemented toward artificial (photo)catalysis, especially in the design of molecular electrocatalysts, most reports focus on inorganic systems. In addition to coordination complex catalysts and natural archetypes, (semi-)organic (hybrid) materials have emerged in the field of catalysis.[3] The modularity and amenability displayed by these materials offer a fertile ground for integration in catalytic schemes, which have led to rapid developments in organic photo- and electrochemistry.[4]

Here, we summarize the progress toward photo- and electro-catalysis for fuels brought through organic design, organized according to molecular and polymeric concepts. Although the synthetic strategies described in this mini-review focus on the fuel forming half-reaction, analogous design can also be employed in water oxidation catalysis.

[b] Department Chemie
Technische Universität München
Lichtenbergstraße 4, 85747 Garching, Germany
E-mail: julien.warnan@tum.de
[a] Department of Chemistry
University of Cambridge
Lensfield Road, Cambridge CB2 1EW, UK
E-mail: reisner@ch.cam.ac.uk

Julien Warnan is a Junior Group Leader at the Chair of Inorganic & Metal-Organic Chemistry at the Technical University (TU) of Munich (Germany). He obtained a Ph.D. in organic chemistry in 2012 from the Université de Nantes (France). After postdoctoral tenures at King Abdullah University of Science and Technology (Saudi Arabia) and the University of Cambridge (UK), he joined TU Munich in 2019. His current research is focused on the development of organic chromophores, polymer systems, and hybrid materials toward solar-driven fuel synthesis.

Erwin Reisner is Professor of Energy and Sustainability at the University of Cambridge and a Fellow of St. John's College (UK). His laboratory explores the interface of chemical biology, synthetic chemistry, materials science, and engineering relevant to the development of solar-driven processes for the sustainable synthesis of fuels and chemicals. He also chairs the Cambridge Creative Circular Plastics Centre (CirPlas) and the UK Solar Fuels Network (SFN), which coordinates the national activities in artificial photosynthesis.

2. Discrete Molecular Systems

2.1. Ligand Design for Catalysts

The [NiFe]- or [FeFe]-active site in H_2ase and the O_2-evolving [$CaMn_4$]-cluster in Photosystem II (PSII) inspired the development of early structural biomimetics as *molecular catalysts*.[5] Catalysts were initially designed to mimic the first coordination sphere of the enzyme active site, which led to Fe_2S_2-type HECs delivering modest performances,[5f, 6] and having the propensity to decompose into highly active particles.[7] Tuning the ligands' substituents to affect the electronic density and electrochemical properties was also extensively investigated.[5e, 6c] A more recent approach is to innovate modulation of the second and outer coordination spheres of the metal center with organic residues in an attempt to replicate the multifunctionality found in enzymes (Fig. 1).[6c, 8]

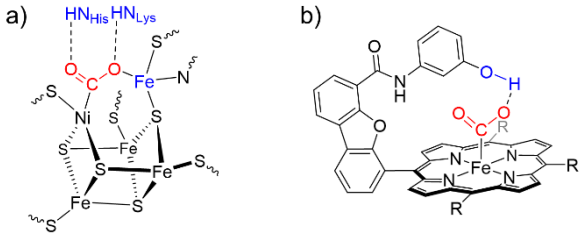

Figure 1. (a) [NiFe] carbon monoxide dehydrogenase active site[9] and (b) synthetic Fe-porphyrin[10] with bound CO_2 (in red) stabilized by outer coordination sphere interactions (in blue).

A class of Ni-containing HECs containing a P_2N_2 ligand (Dubois catalyst) displays high activities due to pendant basic tertiary amines that promote proton transfer.[11] HEC **1** with

further arginine (Arg) residues displayed reversible H_2 production/oxidation in acidic aqueous solutions (Fig. 2).[8c] The high turnover frequency (TOF) of 300 s^{-1} was attributed to Arg-Arg interactions that aid positioning of the pendant-amine groups in close proximity to the Ni center.

Tuning porphyrin ligands to improve the performance of a CO_2 reduction catalyst (CRC) was demonstrated with Fe-tetraphenylporphyrins (TPPs).[8d, 10, 12] Fe-TPPs display a catalytic onset potential (E_{cat}) of −1.40 V vs standard hydrogen electrode (SHE) in *N*,*N*-dimethylformamide (DMF).[12] The catalytic performance were optimized by stabilization of the initial Fe^0–CO_2 adduct upon addition of positively charged *N*,*N*,*N*-trimethylanilinium groups in the *ortho* position of the four phenyl groups in **2** (Fig. 2). This modification resulted in a more anodic E_{cat} of −0.95 V vs SHE with a 3-fold greater catalytic current than the corresponding "*para*" catalyst, while also delivering high Faradaic efficiencies (FEs) toward CO with limited degradation over 84 h of electrolysis in DMF containing phenol and H_2O.[8d] The catalysis-enhancing effect was attributed to Coulombic interactions of the positively charged moieties with the carboxylate borne from the Fe^0-CO_2 adduct.

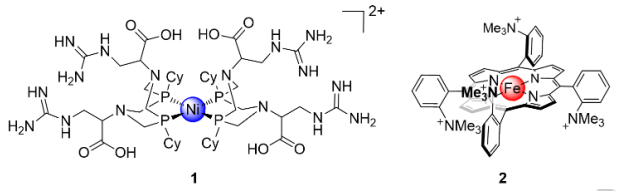

Figure 2. Catalysts with engineered ligands to stabilize reaction intermediates via secondary coordination sphere interactions.

Other concepts to improve performance have been reviewed elsewhere and include (non-exhaustively): modulating steric hindrance around the metal core,[13] isolating catalysts on surfaces via anchoring groups,[14] providing Brønsted acid groups to deliver proton relays,[8b] H-bond and multimetallic systems for electrostatic stabilization of CO_2-bonded intermediates,[15] and tailored CO_2-fitting clefts.[10]

Importantly, as water oxidation represents a scalable and readily available source of electrons for (solar) fuels production, many molecular catalysts for the oxygen evolution reaction have been developed with ligand design toward modulating the catalyst's outer coordination sphere also representing an active area of research.[5a, 16] In particular, Ru coordination complexes currently display benchmark performance and more in-depth reviews on this topic can be found elsewhere.[17]

2.2. Dyes

Photosensitizers (PSs) can harvest light to drive a suitable electrocatalyst for solar fuel synthesis. Common homogeneous photocatalytic systems employ commercial dyes, *e.g.*, Ir and Ru complexes, that are regenerated by a sacrificial electron donor (SED). Purely organic PSs, now ubiquitous in dye-sensitized solar cells (DSCs), have been much less investigated for the demanding requirements of artificial photosynthesis such as aqueous conditions and endergonic multi-electron processes.[18] Common limitations include their lack of solubility in aqueous media, modest stability and short-lived excited states that impede diffusional ET. Building on chromophoric units, these drawbacks can be overcome by molecular engineering to yield suitable PSs (Fig. 3).

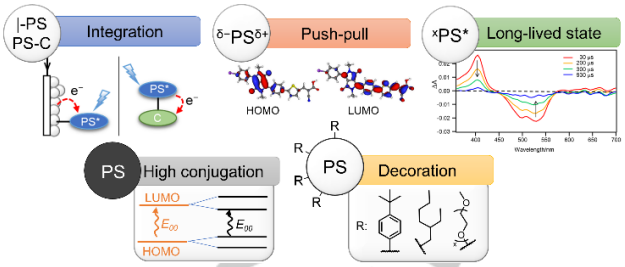

Figure 3. Examples of properties implemented in chromophores toward optimized PSs (C = catalyst). Adapted with permission from ref. [19] and [20]. Copyright (2011 and 2018) Elsevier and American Chemical Society.

For instance, triazatriangulenium **3** (Fig. 4) displays intense visible-light absorption (λ_{max} = 530 nm; ε = 8800 M^{-1} cm^{-1}) with a relatively long excited-state lifetime of its singlet state (14 ns at pH 4.5).[20] This allows in solution for a diffusion-controlled reductive quenching by ascorbic acid (AA) to generate the organic radical $\mathbf{3}^{\bullet-}$ with excellent stability due to the planar scaffold incorporating three electron-donating nitrogen atoms for delocalization of the radical. As a result, efficient ET to a molecular Co HEC was observed, delivering a PS-based turnover number (TON_{PS}) of ~100 (limited by the HEC's stability).

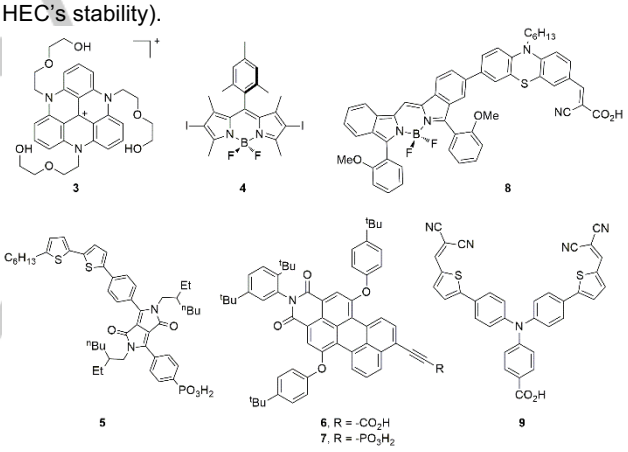

Figure 4. Organic PSs used in photocatalysis.

An alternative PS-design strategy to improve intermolecular ET is the promotion of intersystem crossing toward a long-lived triplet state. Halogenation of a borondipyrromethene PS (bodipy) yields diiodide-bearing **4** (Fig. 4) that has a considerably shorter fluorescence lifetime than the corresponding iodine-free PS (0.13 vs 6.0 ns, respectively), indicating fast intersystem crossing.[21] PS **4** reached a TON_{PS} of 600 when employed at low concentrations with a molecular Co HEC and triethanolamine (TEOA) as a SED in acetonitrile under Xe/Hg lamp irradiation.

Organic dyes have also been involved in colloidal dye-sensitized SC photocatalysis (DSP) systems toward H_2 evolution and CO_2 reduction (Fig. 5a).[22] Building upon DSC principles, DSP systems are assembled through attachment of an anchor-bearing PS to the surface of a SC particle, together with a co-attached catalyst.[18a, 22a] The SC delivers dual

functionality as it provides as a scaffold for immobilization to enable fast charge separation and accumulation of multiple long-lived charges in the SC to drive catalysis. The regeneration of the photoionized PS generally relies on a SED.

A series of diketopyrrolopyrrole (DPP) dyes with modulated energetic and non-energetic parameters (*e.g.*, steric hindrance, position and nature of the solubilizing side chains) were studied in DSP systems.[23] When attached to platinized TiO_2 and placed under simulated sunlight, PS **5** (Fig. 4) delivered a performance (TON_{PS} in **5**|TiO_2|Pt ~2700) superior even to the corresponding phosphonic acid-bearing Ru trisbipyridine-based assembly. The performance of the PS in DSP systems was shown to ultimately depend on the orthogonal adequacy of PS design and external parameters (pH, SED, chemical catalyst and mechanistic details).

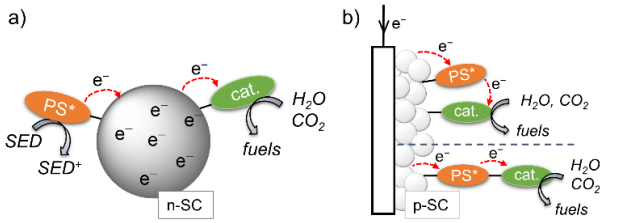

Figure 5. Schematic representation of (a) colloidal DSP and (b) DSPC schemes, with a PS and catalyst (cat.) or a PS-cat. dyad co-anchored onto a SC electrode.

A series of hydrophobic perylene monoimide (PMI) dyes were functionalized with five different anchoring groups: carboxylic acid, phosphonic acid, acetylacetone, pyridine-2,6-dicarboxylic acid and hydroxyquinoline. These PSs were investigated in DSP using platinized TiO_2 nanoparticles for H_2 evolution in water.[24] The CO_2H-bearing PS **6** (Fig. 4) delivered the highest performance in acidic and neutral pH with a stability beyond 3 days and a TON_{PS} of ~11,000. The activity decreased at higher pH due to desorption of the PS from the SC surface. In contrast, albeit yielding modest activity, the phosphonic acid-bearing PS **7** (Fig. 4) enables good stability due to the anchoring group's better resistance to hydrolysis. These results highlight an ongoing challenge in DSP, where electron injection-promoting properties are not yet readily compatible with robust anchoring.

The tunable electronic properties of organic chromophores allow their use for the absorption and conversion of low-energy photons. PS **8** (Fig. 4) shows the extended conjugation of a bodipy to a phenothiazine, with its donor-π conjugated linker-acceptor (D-π-A) organization leading to strong panchromatic absorption up to 700 nm with λ_{max} = 638 nm (ε = 123,000 M^{-1} cm^{-1}). Attachment of **8** on platinized hierarchical porous TiO_2 resulted in a DSP system toward H_2 evolution, with a TON_{PS} of 11,100 after 10 h of irradiation (λ > 400 nm, 100 mW cm^{-2}) in the presence of AA as SED. An apparent quantum yield (QY) of 1.0% at 750 nm was recorded.[25]

Overcoming the parasitic, fast electron recombination in PS-catalyst systems as well as suppressing the need for a SED are current challenges in colloidal and homogeneous schemes. Anchoring a dye and catalyst onto a p-type SC (p-SC) electrode to produce a dye-sensitized photocathode (DSPC, Fig. 5b) is a promising strategy inspired by p-type DSCs.[3c, 26] PS **9** (Fig. 4) was co-anchored to a nanostructured NiO substrate together with a cobaloxime HEC.[27] The push-pull design in **9** locates the dye's highest occupied molecular orbital close to the NiO surface, thereby promoting hole injection and intermolecular ET to the HEC upon photoexcitation. A fully assembled tandem photoelectrochemical cell with a dye-sensitized photoanode demonstrated overall water splitting.[27] Incident photon to current conversion efficiency analysis identified the photocathode as the overall system's bottleneck, ascribed to the limitations of NiO (*e.g.*, short hole diffusion length). Alternative p-SCs such as $CuCrO_2$ (combined with PSs **5** and **7**) and $LaFeO_3$ have recently been proposed as a potential replacement for NiO.[28]

2.3. Molecular Electro- and Photo-catalysis

Photocatalysts require structures with high molar absorption and a reactive catalytic center.[29] The difficulty of combining these two properties in one discrete molecule led to the development of architectures that covalently or supramolecularly bind a dye to an electrocatalyst,[30] where the photoexcited PS triggers intramolecular ET to the catalyst site. Such dyads often rely on a precious metal-based PS, but organic chromophores are emerging.

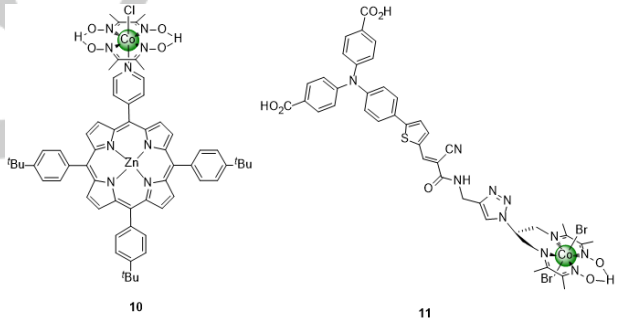

Figure 6. Photocatalysts based on transition metal-free PSs.

Cobaloxime-based dyads are usually assembled from the HEC unit bound axially to a pyridine-functionalized PS. An example is the Zn-porphyrin-cobaloxime dyad **10** (Fig. 6), which photogenerated a TON_{H2} of 22 after 5 h irradiation (λ > 400 nm) in H_2O:tetrahydrofuran (THF) (1:4) with triethylamine (TEA) as SED.[30a] No H_2 was detected when using Zn-porphyrin not bound to the cobaloxime.

A photocatalyst composed of a cobaloxime HEC linked to the carboxylate anchor-bearing PS **11** (Fig. 6) was used as a dyad in a DSPC (PS-cat., Fig. 5b).[30d] The PS's push-pull design locates the lowest unoccupied molecular orbital close to the HEC and thereby promotes its intramolecular reduction upon irradiation. As a result, a NiO|**11** DSPC displayed an early photocurrent onset potential of +0.61 V vs SHE, and chronoamperometry at −0.18 V vs SHE in pH 5.5 under simulated solar irradiation resulted in a FE_{H2} of 8−10%.

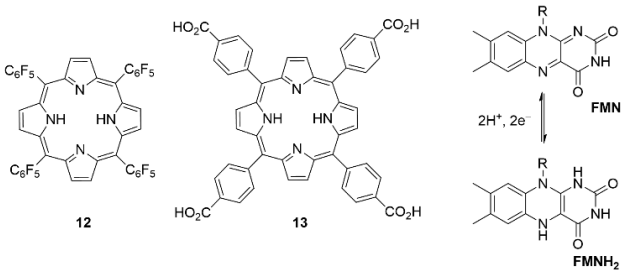

Figure 7. Metal-free compounds for electro- and photo-driven fuel production.

Another challenge for metal-free molecular systems is delivering fuel production activity.[31] A free-base porphyrin (P2H) bearing four electron-withdrawing meso-tetra(pentafluorophenyl) groups (**12**, Fig. 7) achieved H_2 production.[32] Cyclic voltammetry conducted in THF featured two reversible 1-e$^-$ reductions at $E_{1/2}$ = −1.14 and −1.54 V vs ferrocene/ferrocenium (Fc/Fc$^+$). Upon addition of tosic acid, the first reduction wave remained unchanged, while an enhanced wave appears at −1.31 V vs Fc/Fc$^+$, indicating that protonation of the porphyrin occurs in the cavity after the first reduction (Fig. 8). H_2 evolution was observed during bulk chronoamperometric experiments at −1.7 V vs Fc/Fc$^+$, with 90% FE after 40 min and a calculated TON <1.

Another P2H (**13**, Fig. 7) is capable of photo-catalyzing the production of H_2O_2 from O_2 when immobilized on NiO.[33] H_2O_2 has potential as a liquid fuel with an energy density comparable to that of compressed H_2. Bulk electrolysis of NiO|**13** at ~+0.20 V vs SHE (pH 6) under 623 nm LED irradiation for 24 h resulted in near-unity FE and a TON >12,000. The production of H_2O_2 was attributed to the light-driven reduction of O_2 by **13** into the superoxide radical anion $O_2^{\bullet-}$, which further disproportionates into H_2O_2.

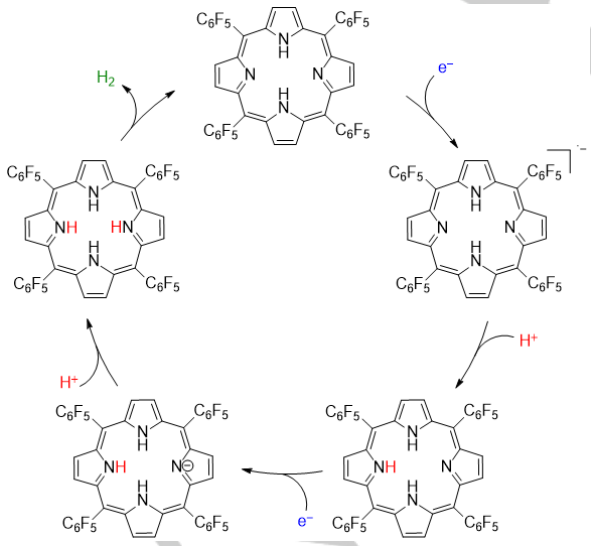

Figure 8. Proposed H_2 evolution mechanism with **12**.[32]

Flavins are organic electro- and photo-catalyst studied toward chemical and water oxidation that commonly uses O_2 as the final electron acceptor in order to produce H_2O_2.[34] Similar to quinone, flavin-derivatives exist in three redox states: neutral (flavin-quinone **FMN**, Fig. 7), 1e$^-$-reduced, and 2e$^-$-reduced (flavin-hydroquinone, **FMNH$_2$**). Upon irradiation with blue light, the **FMN** chromophores form a singlet excited state, a potent oxidant with E(FMN*/FMN$^{\bullet-}$) = +1.53 V vs SHE. Rapid intersystem crossing (7.8 ns in water) also produces a triplet state that triggers ET. **FMNH$_2$** is usually ultimately oxidized to **FMN** in presence of O_2. Alternative mechanisms could be promoted; for instance, with FMN* converting $^3O_2$ into the reactive $^1O_2$ species.[34c]

3. Polymeric Systems

Whilst Nafion® remains the most commonly used polymer, alternatives are quickly being developed for solar fuel applications. Electropolymerization was employed early as a mean to surface anchor molecular catalysts via pyrrole, vinyl and methacrylate groups in water oxidation, proton and CO_2 reduction.[35] Recent reports have considerably expanded the scope of bespoke polymers toward solar fuel production with applications ranging from scaffolds and catalysts to PSs.

3.1. Scaffolds for Electrocatalysts

The active sites of enzymes are embedded into polypeptide scaffolds. Synthetic polymeric matrices can similarly integrate HECs or CRCs to provide better stability, and functionalities to stabilize catalytic intermediates or allow for surface anchoring.[36]

An amine-containing metallopolymer **14** (Fig. 9) derived from 2-(dimethylamino)ethylmethacrylate and a Fe_2S_2-type HEC operates in pH neutral aqueous solution with high current densities, a TON of 2.6×10^4, an operational lifetime of 6 d and even retained activity under aerobic conditions. The high performance is possibly due to the protonation of amine side-chains that facilitates proton transport to the Fe-catalyst while shielding it from O_2 reduction products.[36d]

A cobaloxime HEC was integrated into a cross-linked copolymer via a pyridine ligand that also contained pyrene and amphiphilic ethylene glycol groups (**15**, Fig. 9). Interfacing this structure with carbon nanotubes resulted in a standalone electrode achieving higher TONs and stability compared to an electrode with the immobilized monomeric cobaloxime HEC. The improved performance was attributed to entrapment of the otherwise labile Co HEC in the polymeric matrix and improved proton transport from the ethylene glycol moieties. This work highlights the potential benefits by considering the choice of co-monomers, independent of the HEC unit itself.[36a]

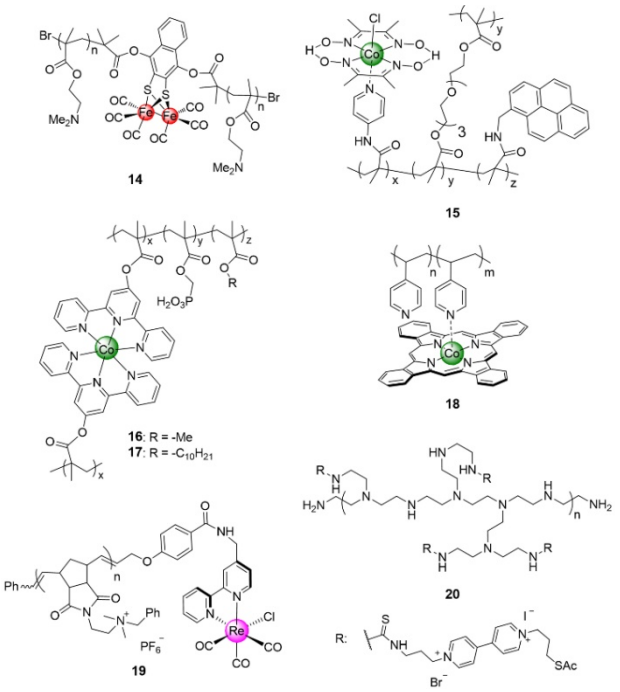

Figure 9. Scaffolding polymers for electrocatalytic systems.

A similar copolymeric approach was applied toward CO-selective CO_2 reduction using a Co bis(terpyridine) CRC. Two coordination copolymers were prepared comprising the CRC, phosphonic acid anchoring groups, and either a methyl or decyl moiety to tune hydrophobicity surrounding the catalyst core in **16** and **17**, respectively (Fig. 9 and 10a). After integration of the copolymers into bespoke inverse opal TiO_2 electrodes (pore Ø = 750 nm, Fig. 10b), electrolysis demonstrated higher selectivity toward CO vs H_2 for the more hydrophobic, decyl-based copolymer, highlighting the possibilities for improved product selectivity offered by tuning the catalyst's outer sphere environment.[36e]

Poly-4-vinylpyridine coordinated to a Co phthalocyanine (CoPc) in sub-stoichiometric conditions resulted in polymer **18** (Fig. 9) that was interfaced with graphite electrodes. A better electrolysis performance for CO_2 reduction was achieved compared to the corresponding pyridine-coordinated, molecular CoPc, which was attributed to outer sphere effects of uncoordinated pyridines.[36b]

A series of polymeric frameworks with positively charged ammonium salts, phenyl, or negatively charged trifluoroborate group were designed to alter the catalytic activity of a covalently bound Re CRC.[36c] Electrochemical studies in organic solvent showed that the quaternary ammonium-containing polymers **19** (Fig. 9) have a significantly lower E_{cat} toward CO evolution (~300 mV) compared to the free, molecular catalyst. In contrast, the trifluoroborate polymers displayed a negative shift in potential and catalytic activity was not observed. This illustrates how a charged polymeric framework can influence the catalytically active species without changing the direct microenvironment around the reactive center.

Using a semi-biological approach,[37] a multifunctional polymer was employed as a hydrogel to provide stabilization and entrapment to an O_2-sensitive [NiFe]-H_2ase toward biofuel cell applications.[37a, 37d] The polyamine-based polymer **20** (Fig. 9) was synthesized from a branched poly(iminoethylene) functionalized with electroactive methyl viologen (MV) units.[37a] The MV units in **20** act as an electron relay for enzymatic catalysis and reduce O_2 to protect the H_2ase. A few micrometer-thick polymer film is sufficient to protect the H_2ase without compromising the current generation efficiency.[37d]

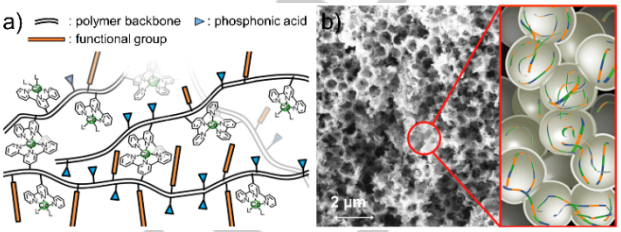

Figure 10. (a) Schematic representation of **16** and **17** and (b) scanning electron microscopy image of inverse opal TiO_2 and schematic of polymer chains embedded in the porous scaffold. Reprinted with permission from ref. [36e]. Copyright (2019) John Wiley and Sons.

A phenothiazine-based polymer was employed to wire PSII to a porous electrode for photoelectrocatalytic water oxidation.[37b] Integration of PSII via a polymer-matrix to a dye-sensitized photoanode (using PS **5**) enabled unassisted overall water splitting with a cathode containing H_2ase.[37c]

3.2. Polymeric Dyes and Photocatalysts

Light harvesting and charge conducting SCs are ubiquitous in lightweight optoelectronics applications and typically produced from conjugated polymers (CPs). CPs can be produced under mild conditions with molecularly tunable optoelectronic and physicochemical properties.[38] Recently, they have also emerged as promising materials for photocatalytic fuel production delivering high catalytic activities, often when combined with added or residual Pd/Pt nanoparticles.[3d] In some cases, thorough metal removal and purification has been shown to eliminate activity, demonstrating that residual Pd – even at ppm-level (e.g. from cross-coupling reactions) – plays a significant role in the H_2 evolution abilities of some polymers.[39]

CPs have evolved from linear polymers to non-crystalline microporous polymer networks, carbon nitrides and carbon dots, polymer dots (Pdots) and covalent organic frameworks (COFs) (Fig. 11).[40] Carbon nitride derivatives (and other triazine-based systems) and carbon dots (along with other carbon nanoparticles) are attracting much attention,[41] and they can be fabricated from purely organic precursors (*e.g.,* melamine, urea, cyanamide, citric acid and aspartic acid) via pyrolysis and solvothermal procedures at relatively high temperatures.[3b, 41a, 41c, 42] Modulation of their photocatalytic activity generally involves solid-state approaches to introduce morphological alteration, doping and composite construction.[3b, 41b] Given that the synthetic procedures, tuning approaches and properties of these materials differ significantly from the molecularly-defined polymeric materials described in this section, we will not examine them further. Reviews on carbon nitrides and carbon dots can be found elsewhere.[3b, 42a] Hereafter, we focus on polymer engineering strategies to

enhance activities, including improved light-harvesting properties, porosity and crystallinity.

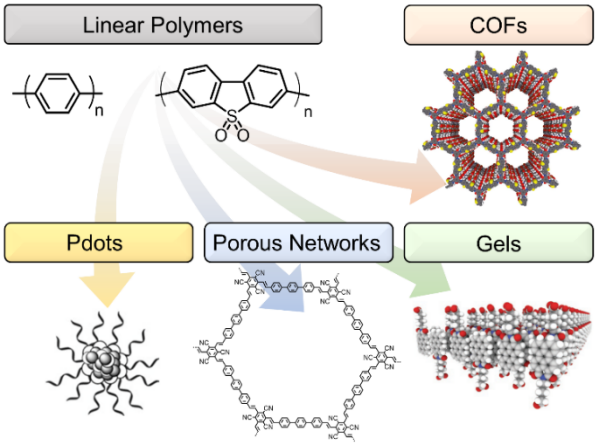

Figure 11. Evolution from linear polymeric aggregates to controlled 2D/3D polymeric architectures. Adapted with permission from ref. [43]. Copyright (2016, 2014 and 2018) John Wiley and Sons and Springer Nature.

CPs offer the possibility of fine-tuning SC properties such as the energy levels and resulting optical band gap (E_g), through the selection of monomeric building blocks and via modular polymerization strategies. An early report showed that poly(*p*-phenylene) (PPP, Fig. 12a) acts as a photocatalyst for H_2 evolution, despite showing low activity and requiring UV irradiation. The E_g could be reduced from 2.9 to 2.7 eV (for PPP and **21**, respectively) with the introduction of a dibenzo[*b*,*d*]thiophene sulfone moiety and then further to 2.1 eV upon introduction of planarizing ethynyl groups in **22** (Fig. 12a).[40a, 44] The smaller E_g combined with accelerated charge separation allowed for an increase in the photocatalytic rate from 1492 to 6023 $\mu mol_{H2}\ h^{-1}\ g^{-1}$ in the presence of a SED.

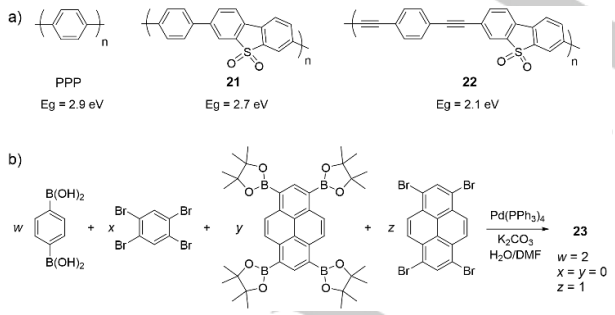

Figure 12. Tuning the bandgap in (a) linear and (b) 3D microporous CPs.

This strategy was also employed in 3D microporous CPs, where high surface area polymers were prepared by adjusting the ratio of four monomers (Fig. 12b).[45] The corresponding E_g thereby gradually decreased from 2.95 to 1.94 eV following an increase in pyrene content.[46] In the absence of an externally added metal catalyst, the polymers showed a gradually enhanced photoactivity for H_2 evolution with an optimal E_g of 2.33 eV for **23**. Polymer **23**, obtained with a ratio of 2:1 for 1,4-benzene diboronic acid:1,3,6,8-tetrabromopyrene, exhibited the highest activity of 174 $\mu mol_{H2}\ h^{-1}\ g^{-1}$ (and a mid-range surface area compared to polymers of other ratios). Further reduction in E_g of the polymers led to a lower rate, which was ascribed to increased nonradiative charge recombination in the pyrene-rich polymers.

The high hydrophobicity of CPs commonly results in their aggregation in aqueous solution into a bulk material composed of micrometer-size particles with low surface area (*i.e.*, water-polymer interface) and extended travelling distance for charge carriers. To overcome these issues, porous systems as well as optimized precipitation and gel-promoting methods have been developed.

The length of the π-extended linker affects the porosity of microporous networks synthesized via condensation, as shown in polymers **24**-**27** (Fig. 13).[47] Polymer **24** with a short *para*-phenylene spacer exhibits micropores, whereas **25** and **27** contain longer spacers and subsequently integrate micro- and mesopores. Polymer **26** shows a much broader pore size distribution due to the longest polyphenylene spacer in the polymer network. As a result, the Brunauer-Emmett-Teller (BET) surface areas were 669, 750, 564 and 834 $m^2\ g^{-1}$ for **24**, **25**, **26** and **27**, respectively. Despite their similar E_g, the corresponding photoactivities were 134, 598, 908 and 620 $\mu mol_{H2}\ h^{-1}\ g^{-1}$, respectively, with the highest rate for **26** and ascribed to its nanoparticular morphology, better wettability and large surface area. This highlights the possibility to influence the activity of polymers via fine-tuning of morphological variations.

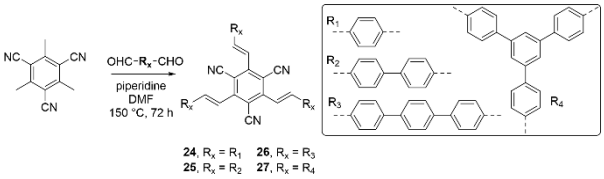

Figure 13. Synthesis of CPs with different porosities.[47]

An alternative approach was developed with the charged amphiphilic PMI dye **28** (Fig. 14), which can self-assemble into ribbon-type supramolecular polymers via hydrophobic collapse.[43a] Moreover, at sufficiently high concentrations, the charged supramolecular polymers produce highly hydrated 3D network hydrogels, which display a high degree of crystallinity. This leads to the PMI losing its individual excitonic character and behaving as an ensemble with photoinduced excitons spreading out over multiple PMI units within the crystalline ribbons. The **28**-based hydrogels formed in presence of poly(diallyldimethylammonium) chloride can host a water-soluble Dubois Ni HEC, ultimately producing a TON_{H2} of ~340 under irradiation in the presence of AA as SED.

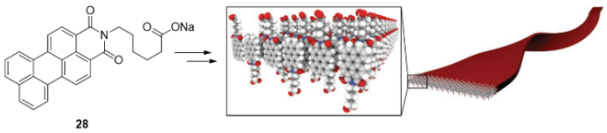

Figure 14. Self-assembled chromophores resulting in a polymer hydrogel. Adapted with permission from ref. [43a]. Copyright (2014) Springer Nature.

Pdots represent another family of organic SC assemblies used in photocatalysis with diameters from 1 to 100 nm.[43b, 48] The smaller size of Pdots compared to bulk materials reduces the distance for photogenerated charges to migrate to the surface, which decreases the recombination probability. A Pdot suspension can be generated by the nano-precipitation method using CPs and a water-soluble polymer. For example, the synthetic polymer **29** and the matrix PS-PEG-CO_2H (Fig. 15) were solubilized in THF and injected into pure water under sonication to produce a suspension after solvent evaporation.[49] Absorption up to 660 nm and a D-A architecture in **29** allowed for an excellent H_2 evolution rate of up to 50 $mmol_{H2}$ h^{-1} g^{-1} under LED irradiation in presence of AA as SED. Although **29** contains traces of Pd (0.1 wt%), theoretical calculations suggested that nitrogen atoms in the benzothiadiazole units may provide the reactive sites for the formation of H_2.

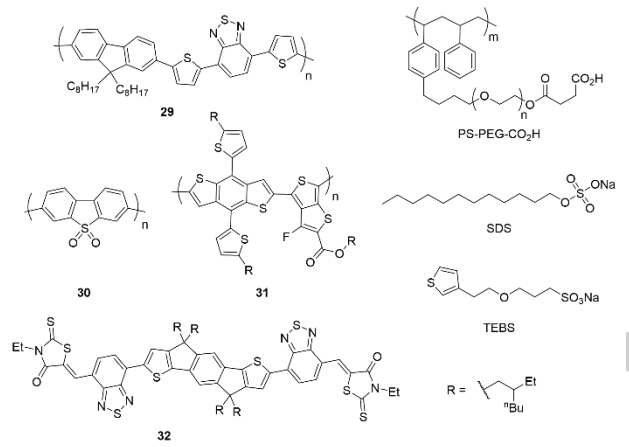

Figure 15. Conjugated architectures and surfactants for Pdot systems.

The linear homopolymer of dibenzo[*b*,*d*]thiophene sulfone **30** produced emulsion particles when synthesized from mini-emulsions of toluene droplets in water with water-stabilizing sodium *n*-dodecyl sulfate (SDS, Fig. 15). The latter exhibited a high surface area of 16 m^2 g^{-1}, contained 0.4 wt% Pd, and produced H_2 with an excellent rate of 61 $mmol_{H2}$ h^{-1} g^{-1} under visible light irradiation in the presence of TEA.[50]

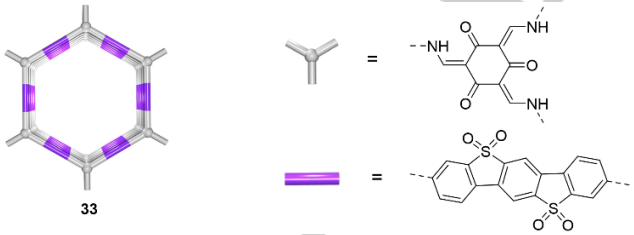

Figure 16. Dibenzo[*b*,*d*]thiophene sulfone-based COF. Adapted with permission from ref. [43c]. Copyright (2018) Springer Nature.

Inspired by bulk heterojunction-based solar cells and emerging examples of photoelectrodes[51], a similar approach was extended to the preparation of heterojunction nanoparticles using a blend of a donor polymer **31** and a non-fullerene acceptor **32**, in the presence of sodium 2-(3-thienyl)ethyloxybutylsulfonate (TEBS) as a stabilizing agent (Fig. 15).[52] The TEBS' affinity of its exposed aromatic units of **32** is believed to control the nanomorphology of these particles into an intermixed D/A blend. SDS, on the other hand, promotes an inefficient core-shell morphology. A 30:70 blend content of **31**:**32** is optimal for efficient exciton dissociation and formation of ~82 nm particles. Following platinization, the photocatalyst displayed a significant H_2 evolution rate of ~64 $mmol_{H2}$ h^{-1} g^{-1} under broadband visible light illumination, and an external QY exceeding 5% from 660 to 700 nm.

Crystallinity can improve the efficiency in conjugated systems as it favors charge transport and separation. COFs are an emerging class of 2D/3D polymers and an example of highly crystalline organic building units combined into extended covalent structures.[53] The well-defined pores, excellent stability and fine-tuned physicochemical properties of COFs make them appealing candidates as PSs and catalysts for fuel production.[54] A dibenzo[*b*,*d*]thiophene sulfone moiety can be integrated into a COF (**33**, Fig. 16), which leads to a high photocatalytic performance of 10 $mmol_{H2}$ h^{-1} g^{-1} when used in presence of Pt and AA as SED.[43c] The COF allows broad visible light absorption (E_g = 1.85 eV) and relatively long excited state lifetimes (τ_{avg} = 5.56 ns) in aqueous suspensions. The high efficiency was ascribed to its good wettability and a large BET area of 1288 m^2 g^{-1} from its 28 Å pore size diameter.

A bipyridine-containing COF was recently post-synthetically modified with a Re complex to afford the photocatalyst **34** (Fig. 17).[55] The latter delivers a CO production rate of 1040 μmol_{CO} g^{-1} h^{-1} with 81% selectivity over H_2, across 17.5 h of illumination (TON_{CO} ~19) in acetonitrile containing TEOA. Computational results support that ET occurs from the light-absorbing COF backbone to the Re CRC upon photoexcitation. Crystallinity and porosity were key factors in the activity of such materials, as an amorphous, low porosity analogue showed almost no catalytic activity.

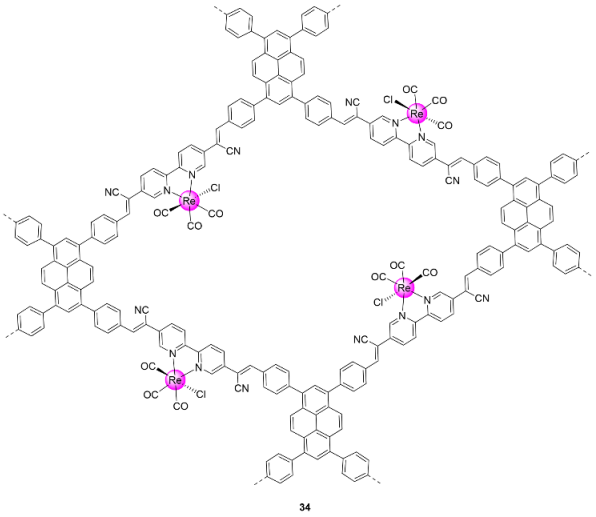

Figure 17. COF for photocatalytic CO_2-to-CO conversion.[55]

4. Conclusions

The development of synthetic organic architectures for fuel catalysis has experienced rapid progress during the past decade and we summarized the wealth of approaches that

originated from integrating organic designs. Tailor-made organic structures have followed several approaches, ranging from small molecules to polymers acting as light harvesters, (photo)catalysts and environment modifiers. Overall, integrations of such organic architectures with inorganic and biological components resulted in innovative hybrids such as DSP, DSPC and COF systems. High performances have already been reached, especially toward photocatalytic H_2 evolution (>60 mmol h^{-1} g^{-1}), making these systems competitive with inorganic counterparts.

The possibility of molecular engineering has played a vital role in achieving these recent developments, with rational design enabling the integration of anchoring abilities, improved reactivity, intense and wide light absorption, high surface area, and efficient charge separation and transport, and so forth. Synergistic combinations of such properties can in principle result in further enhanced catalytic activity. Nevertheless, the structure optimization of one parameter often collaterally impacts other properties, and deconvolution of individual effects remains challenging.

Despite these significant advances, many opportunities for further exploration persist. A better understanding on photocatalytic fuel mechanisms for polymers, COFs and other carbon nanoparticle-based materials is desirable to reach better designs toward higher performance. There is scope for metal-free electrocatalysts and a lack of CO_2-reducing and full water-splitting systems. A particular opportunity lies ahead in the exploration of redox transformations beyond classical solar fuels applications such as organic electro- and photoredox catalysis. The relatively unexplored possibilities offered by tuning the environment around the catalytic center and PS bears many promises and organic chemistry also allows for the development of nanoreactors to enable controlled catalysis in a confined environment.[56] More robust and red-light absorbing PSs[57] are also in demand as well as a better understanding of aqueous media-organic system interfaces and the development of oxidative chemistry.[58] Finally, further integration of organic materials toward biohybrid systems represent another exciting avenue of research.[59] We therefore envision many possibilities to employ organic chemistry in the future development of electro- and photocatalytic systems.

Acknowledgements

Support by the Christian Doppler Research Association (Austrian Federal Ministry of Science, Research and Economy and National Foundation for Research, Technology and Development) and the OMV Group is gratefully acknowledged. JW gratefully acknowledges support from Prof. Roland Fischer and the Deutsche Forschungsgemeinschaft. We appreciate suggestions and comments on the manuscript from Dr. Jane Leung, Dr. Mark Bajada and Mr. Daniel Antón-García.

Keywords: Molecular electronics • Sustainable chemistry • Electrocatalysis • Photocatalysis • Synthesis design

[1] A. Fujishima, K. Honda, *Nature* **1972**, *238*, 37-38.

[2] a) F. A. Armstrong, J. Hirst, *Proc Natl Acad Sci* **2011**, *108*, 14049-14054; b) M. del Barrio, M. Sensi, C. Orain, C. Baffert, S. Dementin, V. Fourmond, C. Léger, *Acc. Chem. Res.* **2018**, *51*, 769-777.

[3] a) V. Balzani, A. Credi, M. Venturi, *ChemSusChem* **2008**, *1*, 26-58; b) W.-J. Ong, L.-L. Tan, Y. H. Ng, S.-T. Yong, S.-P. Chai, *Chem. Rev.* **2016**, *116*, 7159-7329; c) P. Xu, N. S. McCool, T. E. Mallouk, *Nano Today* **2017**, *14*, 42-58; d) C. Dai, B. Liu, *Energy Environ. Sci.* **2020**, *13*, 24-52.

[4] a) R. Brimioulle, D. Lenhart, M. M. Maturi, T. Bach, *Angew. Chem. Int. Ed.* **2015**, *54*, 3872-3890; b) N. A. Romero, D. A. Nicewicz, *Chem. Rev.* **2016**, *116*, 10075-10166; c) E. Reisner, *Angew. Chem. Int. Ed.* **2019**, *58*, 3656-3657.

[5] a) S. W. Gersten, G. J. Samuels, T. J. Meyer, *J. Am. Chem. Soc.* **1982**, *104*, 4029-4030; b) D. J. Darensbourg, J. H. Reibenspies, C.-H. Lai, W.-Z. Lee, M. Y. Darensbourg, *J. Am. Chem. Soc.* **1997**, *119*, 7903-7904; c) T. Glaser, T. Beissel, E. Bill, T. Weyhermüller, V. Schünemann, W. Meyer-Klaucke, A. X. Trautwein, K. Wieghardt, *J. Am. Chem. Soc.* **1999**, *121*, 2193-2208; d) J. Windhager, R. A. Seidel, U.-P. Apfel, H. Görls, G. Linti, W. Weigand, *Chem. Biodiversity* **2008**, *5*, 2023-2041; e) F. Gloaguen, T. B. Rauchfuss, *Chem. Soc. Rev.* **2009**, *38*, 100-108; f) C. Tard, C. J. Pickett, *Chem. Rev.* **2009**, *109*, 2245-2274.

[6] a) F. Gloaguen, J. D. Lawrence, T. B. Rauchfuss, *J. Am. Chem. Soc.* **2001**, *123*, 9476-9477; b) S. Ott, M. Kritikos, B. Akermark, L. Sun, R. Lomoth, *Angew. Chem. Int. Ed.* **2004**, *43*, 1006-1009; c) K. E. Dalle, J. Warnan, J. J. Leung, B. Reuillard, I. S. Karmel, E. Reisner, *Chem. Rev.* **2019**, *119*, 2752-2875.

[7] D. Heift, *Inorganics* **2019**, *7*, 75.

[8] a) A. Le Goff, V. Artero, B. Jousselme, P. D. Tran, N. Guillet, R. Métayé, A. Fihri, S. Palacin, M. Fontecave, *Science* **2009**, *326*, 1384-1387; b) C. H. Lee, D. K. Dogutan, D. G. Nocera, *J. Am. Chem. Soc.* **2011**, *133*, 8775-8777; c) A. Dutta, D. L. DuBois, J. A. S. Roberts, W. J. Shaw, *Proc. Natl. Acad. Sci.* **2014**, *111*, 16286-16291; d) I. Azcarate, C. Costentin, M. Robert, J.-M. Savéant, *J. Am. Chem. Soc.* **2016**, *138*, 16639-16644; e) A. W. Nichols, C. W. Machan, *Front. Chem.* **2019**, *7*, 10.3389/fchem.2019.00397.

[9] J. H. Jeoung, H. Dobbek, *Science* **2007**, *318*, 1461-1464.

[10] C. G. Margarit, C. Schnedermann, N. G. Asimow, D. G. Nocera, *Organometallics* **2019**, *38*, 1219-1223.

[11] S. Wiese, U. J. Kilgore, M.-H. Ho, S. Raugei, D. L. DuBois, R. M. Bullock, M. L. Helm, *ACS Catal.* **2013**, *3*, 2527-2535.

[12] M. Hammouche, D. Lexa, J. M. Savéant, M. Momenteau, *J. Electroanal. Chem. Interfacial. Electrochem.* **1988**, *249*, 347-351.

[13] M. D. Sampson, A. D. Nguyen, K. A. Grice, C. E. Moore, A. L. Rheingold, C. P. Kubiak, *J. Am. Chem. Soc.* **2014**, *136*, 5460-5471.

[14] B. Reuillard, K. H. Ly, T. E. Rosser, M. F. Kuehnel, I. Zebger, E. Reisner, *J. Am. Chem. Soc.* **2017**, *139*, 14425-14435.

[15] E. Haviv, D. Azaiza-Dabbah, R. Carmieli, L. Avram, J. M. L. Martin, R. Neumann, *J. Am. Chem. Soc.* **2018**, *140*, 12451-12456.

[16] a) R. Matheu, M. Z. Ertem, J. Benet-Buchholz, E. Coronado, V. S. Batista, X. Sala, A. Llobet, *J. Am. Chem. Soc.* **2015**, *137*, 10786-10795; b) N. Vereshchuk, R. Matheu, J. Benet-Buchholz, M. Pipelier, J. Lebreton, D. Dubreuil, A. Tessier, C. Gimbert-Suriñach, M. Z. Ertem, A. Llobet, *J. Am. Chem. Soc.* **2020**, *142*, 5068-5077.

[17] a) R. Matheu, M. Z. Ertem, C. Gimbert-Suriñach, X. Sala, A. Llobet, *Chem. Rev.* **2019**, *119*, 3453-3471; b) B. Zhang, L. Sun, *J. Am. Chem. Soc.* **2019**, *141*, 5565-5580.

[18] a) A. Hagfeldt, G. Boschloo, L. Sun, L. Kloo, H. Pettersson, *Chem. Rev.* **2010**, *110*, 6595-6663; b) Y. Ooyama, Y. Harima, *ChemPhysChem* **2012**, *13*, 4032-4080; c) F. Bella, C. Gerbaldi, C. Barolo, M. Grätzel, *Chem. Soc. Rev.* **2015**, *44*, 3431-3473.

[19] J. Warnan, L. Favereau, Y. Pellegrin, E. Blart, D. Jacquemin, F. Odobel, *J. Photochem. Photobiol., A* **2011**, *226*, 9-15.

[20] R. Gueret, L. Poulard, M. Oshinowo, J. Chauvin, M. Dahmane, G. Dupeyre, P. P. Lainé, J. Fortage, M.-N. Collomb, *ACS Catal.* **2018**, *8*, 3792-3802.

[21] R. P. Sabatini, B. Lindley, T. M. McCormick, T. Lazarides, W. W. Brennessel, D. W. McCamant, R. Eisenberg, *J. Phys. Chem. B* **2016**, *120*, 527-534.

[22] a) J. Willkomm, K. L. Orchard, A. Reynal, E. Pastor, J. R. Durrant, E. Reisner, *Chem. Soc. Rev.* **2016**, *45*, 9-23; b) Y. Kou, S. Nakatani, G. Sunagawa, Y. Tachikawa, D. Masui, T. Shimada, S. Takagi, D. A. Tryk, Y. Nabetani, H. Tachibana, H. Inoue, *J. Catal.* **2014**, *310*, 57-66.

[23] J. Warnan, J. Willkomm, J. N. Ng, R. Godin, S. Prantl, J. R. Durrant, E. Reisner, *Chem. Sci.* **2017**, *8*, 3070-3079.

[24] J. Warnan, J. Willkomm, Y. Farré, Y. Pellegrin, M. Boujtita, F. Odobel, E. Reisner, *Chem. Sci.* **2019**, *10*, 2758-2766.

[25] O. Suryani, Y. Higashino, H. Sato, Y. Kubo, *ACS Appl. Energy Mater.* **2019**, *2*, 448-458.
[26] C. Decavoli, C. L. Boldrini, N. Manfredi, A. Abbotto, *Eur. J. Inorg. Chem.* **2020**, *2020*, 978-999.
[27] F. Li, K. Fan, B. Xu, E. Gabrielsson, Q. Daniel, L. Li, L. Sun, *J. Am. Chem. Soc.* **2015**, *137*, 9153-9159.
[28] a) F. Li, R. Xu, C. Nie, X. Wu, P. Zhang, L. Duan, L. Sun, *Chem. Commun.* **2019**, *55*, 12940-12943; b) C. E. Creissen, J. Warnan, E. Reisner, *Chem. Sci.* **2018**, *9*, 1439-1447; c) C. E. Creissen, J. Warnan, D. Antón-García, Y. Farré, F. Odobel, E. Reisner, *ACS Catal.* **2019**, *9*, 9530-9538.
[29] a) R. Henning, W. Schlamann, H. Kisch, *Angew. Chem. Int. Ed.* **1980**, *19*, 645-646; b) J. Hawecker, J.-M. Lehn, R. Ziessel, *J. Chem. Soc., Chem. Commun.* **1983**, *0*, 536-538; c) H. Rao, L. C. Schmidt, J. Bonin, M. Robert, *Nature* **2017**, *548*, 74-77.
[30] a) P. Zhang, M. Wang, C. Li, X. Li, J. Dong, L. Sun, *Chem. Commun.* **2010**, *46*, 8806-8808; b) A. M. Kluwer, R. Kapre, F. Hartl, M. Lutz, A. L. Spek, A. M. Brouwer, P. W. N. M. van Leeuwen, J. N. H. Reek, *Proc. Natl. Acad. Sci.* **2009**, *106*, 10460–10465; c) G.-G. Luo, K. Fang, J.-H. Wu, J.-C. Dai, Q.-H. Zhao, *Phys. Chem. Chem. Phys.* **2014**, *16*, 23884-23894; d) N. Kaeffer, J. Massin, C. Lebrun, O. Renault, M. Chavarot-Kerlidou, V. Artero, *J. Am. Chem. Soc.* **2016**, *138*, 12308-12311.
[31] S. Shima, O. Pilak, S. Vogt, M. Schick, M. S. Stagni, W. Meyer-Klaucke, E. Warkentin, R. K. Thauer, U. Ermler, *Science* **2008**, *321*, 572-575.
[32] Y. Wu, N. Rodríguez-López, D. Villagrán, *Chem. Sci.* **2018**, *9*, 4689-4695.
[33] O. Jung, M. L. Pegis, Z. Wang, G. Banerjee, C. T. Nemes, W. L. Hoffeditz, J. T. Hupp, C. A. Schmuttenmaer, G. W. Brudvig, J. M. Mayer, *J. Am. Chem. Soc.* **2018**, *140*, 4079-4084.
[34] a) E. Mirzakulova, R. Khatmullin, J. Walpita, T. Corrigan, N. M. Vargas-Barbosa, S. Vyas, S. Oottikkal, S. F. Manzer, C. M. Hadad, K. D. Glusac, *Nature Chem.* **2012**, *4*, 794-801; b) P. Dongare, I. MacKenzie, D. Wang, D. A. Nicewicz, T. J. Meyer, *Proc. Natl. Acad. Sci.* **2017**, *114*, 9279-9283; c) W. Zhang, K. L. Carpenter, S. Lin, *Angew. Chem. Int. Ed.* **2020**, *59*, 409-417.
[35] a) S. K. Ibrahim, X. Liu, C. Tard, C. J. Pickett, *Chem. Commun.* **2007**, *0*, 1535-1537; b) A. Krawicz, J. Yang, E. Anzenberg, J. Yano, I. D. Sharp, G. F. Moore, *J. Am. Chem. Soc.* **2013**, *135*, 11861-11868; c) T. Arai, S. Sato, T. Morikawa, *Energy Environ. Sci.* **2015**, *8*, 1998-2002; d) D. L. Ashford, A. M. Lapides, A. K. Vannucci, K. Hanson, D. A. Torelli, D. P. Harrison, J. L. Templeton, T. J. Meyer, *J. Am. Chem. Soc.* **2014**, *136*, 6578-6581.
[36] a) B. Reuillard, J. Warnan, J. J. Leung, D. W. Wakerley, E. Reisner, *Angew. Chem. Int. Ed.* **2016**, *55*, 3952-3957; b) W. W. Kramer, C. C. L. McCrory, *Chem. Sci.* **2016**, *7*, 2506-2515; c) S. Sahu, P. L. Cheung, C. W. Machan, S. A. Chabolla, C. P. Kubiak, N. C. Gianneschi, *Chem.--Eur. J.* **2017**, *23*, 8619-8622; d) W. P. Brezinski, M. Karayilan, K. E. Clary, N. G. Pavlopoulos, S. Li, L. Fu, K. Matyjaszewski, D. H. Evans, R. S. Glass, D. L. Lichtenberger, J. Pyun, *Angew. Chem. Int. Ed.* **2018**, *57*, 11898-11902; e) J. J. Leung, J. A. Vigil, J. Warnan, E. Edwardes Moore, E. Reisner, *Angew. Chem. Int. Ed.* **2019**, *58*, 7697-7701; f) F. Wang, W.-J. Liang, J.-X. Jian, C.-B. Li, B. Chen, C.-H. Tung, L.-Z. Wu, *Angew. Chem. Int. Ed.* **2013**, *52*, 8134-8138.
[37] a) N. Plumeré, O. Rüdiger, A. A. Oughli, R. Williams, J. Vivekananthan, S. Pöller, W. Schuhmann, W. Lubitz, *Nature Chem.* **2014**, *6*, 822-827; b) K. P. Sokol, D. Mersch, V. Hartmann, J. Z. Zhang, M. M. Nowaczyk, M. Rogner, A. Ruff, W. Schuhmann, N. Plumeré, E. Reisner, *Energy Environ. Sci.* **2016**, *9*, 3698-3709; c) K. P. Sokol, W. E. Robinson, J. Warnan, N. Kornienko, M. M. Nowaczyk, A. Ruff, J. Z. Zhang, E. Reisner, *Nat. Energy.* **2018**, *3*, 944-951; d) H. Li, D. Buesen, S. Dementin, C. Léger, V. Fourmond, N. Plumeré, *J. Am. Chem. Soc.* **2019**, *141*, 16734-16742.
[38] H. Bronstein, C. B. Nielsen, B. C. Schroeder, I. McCulloch, *Nat. Rev. Chem.* **2020**, *4*, 66-77.
[39] J. Kosco, M. Sachs, R. Godin, M. Kirkus, L. Francas, M. Bidwell, M. Qureshi, D. Anjum, J. R. Durrant, I. McCulloch, *Adv. Energy Mater.* **2018**, *8*, 1802181.
[40] a) S. Yanagida, A. Kabumoto, K. Mizumoto, C. Pac, K. Yoshino, *J. Chem. Soc., Chem. Commun.* **1985**, 474-475; b) Y. Wang, A. Vogel, M. Sachs, R. S. Sprick, L. Wilbraham, S. J. A. Moniz, R. Godin, M. A. Zwijnenburg, J. R. Durrant, A. I. Cooper, J. Tang, *Nat. Energy.* **2019**, *4*, 746-760.
[41] a) A. Cayuela, M. L. Soriano, C. Carrillo-Carrión, M. Valcárcel, *Chem. Commun.* **2016**, *52*, 1311-1326; b) L. Lin, Z. Yu, X. Wang, *Angew. Chem. Int. Ed.* **2019**, *58*, 6164-6175; c) X. Wang, K. Maeda, A. Thomas, K. Takanabe, G. Xin, J. M. Carlsson, K. Domen, M. Antonietti, *Nat. Mater.* **2009**, *8*, 76-80.
[42] a) G. A. M. Hutton, B. C. M. Martindale, E. Reisner, *Chem. Soc. Rev.* **2017**, *46*, 6111-6123; b) M. Liu, L. Guo, S. Jin, B. Tan, *J. Mater. Chem. A* **2019**, *7*, 5153-5172.
[43] a) A. S. Weingarten, R. V. Kazantsev, L. C. Palmer, M. McClendon, A. R. Koltonow, A. P. S. Samuel, D. J. Kiebala, M. R. Wasielewski, S. I. Stupp, *Nature Chem.* **2014**, *6*, 964-970; b) L. Wang, R. Fernández-Terán, L. Zhang, D. L. A. Fernandes, L. Tian, H. Chen, H. Tian, *Angew. Chem. Int. Ed.* **2016**, *55*, 12306-12310; c) X. Wang, L. Chen, S. Y. Chong, M. A. Little, Y. Wu, W.-H. Zhu, R. Clowes, Y. Yan, M. A. Zwijnenburg, R. S. Sprick, A. I. Cooper, *Nature Chem.* **2018**, *10*, 1180-1189.
[44] a) R. S. Sprick, B. Bonillo, R. Clowes, P. Guiglion, N. J. Brownbill, B. J. Slater, F. Blanc, M. A. Zwijnenburg, D. J. Adams, A. I. Cooper, *Angew. Chem. Int. Ed.* **2016**, *55*, 1792-1796; b) X.-H. Zhang, X.-P. Wang, J. Xiao, S.-Y. Wang, D.-K. Huang, X. Ding, Y.-G. Xiang, H. Chen, *J. Catal.* **2017**, *350*, 64-71.
[45] J.-S. M. Lee, A. I. Cooper, *Chem. Rev.* **2020**, *120*, 2171-2214.
[46] R. S. Sprick, J.-X. Jiang, B. Bonillo, S. Ren, T. Ratvijitvech, P. Guiglion, M. A. Zwijnenburg, D. J. Adams, A. I. Cooper, *J. Am. Chem. Soc.* **2015**, *137*, 3265-3270.
[47] S. Bi, Z.-A. Lan, S. Paasch, W. Zhang, Y. He, C. Zhang, F. Liu, D. Wu, X. Zhuang, E. Brunner, X. Wang, F. Zhang, *Adv. Funct. Mater.* **2017**, *27*, 1703146.
[48] L. Feng, C. Zhu, H. Yuan, L. Liu, F. Lv, S. Wang, *Chem. Soc. Rev.* **2013**, *42*, 6620-6633.
[49] P. B. Pati, G. Damas, L. Tian, D. L. A. Fernandes, L. Zhang, I. B. Pehlivan, T. Edvinsson, C. M. Araujo, H. Tian, *Energy Environ. Sci.* **2017**, *10*, 1372-1376.
[50] Catherine M. Aitchison, R. S. Sprick, A. I. Cooper, *J. Mater. Chem. A* **2019**, *7*, 2490-2496.
[51] a) T. Bourgeteau, D. Tondelier, B. Geffroy, R. Brisse, C. Laberty-Robert, S. Campidelli, R. de Bettignies, V. Artero, S. Palacin, B. Jousselme, *Energy Environ. Sci.* **2013**, *6*, 2706-2713; b) L. Yao, A. Rahmanudin, N. Guijarro, K. Sivula, *Adv. Energy Mater.* **2018**, *8*, 1802585.
[52] J. Kosco, M. Bidwell, H. Cha, T. Martin, C. T. Howells, M. Sachs, D. H. Anjum, S. Gonzalez Lopez, L. Zou, A. Wadsworth, W. Zhang, L. Zhang, J. Tellam, R. Sougrat, F. Laquai, D. M. DeLongchamp, J. R. Durrant, I. McCulloch, *Nat. Mater.* **2020**, *19*, 559-565.
[53] P. J. Waller, F. Gándara, O. M. Yaghi, *Acc. Chem. Res.* **2015**, *48*, 3053-3063.
[54] H. Wang, H. Wang, Z. Wang, L. Tang, G. Zeng, P. Xu, M. Chen, T. Xiong, C. Zhou, X. Li, D. Huang, Y. Zhu, Z. Wang, J. Tang, *Chem. Soc. Rev.* **2020**, 10.1039/D1030CS00278J.
[55] Z. Fu, X. Wang, A. M. Gardner, X. Wang, S. Y. Chong, G. Neri, A. J. Cowan, L. Liu, X. Li, A. Vogel, R. Clowes, M. Bilton, L. Chen, R. S. Sprick, A. I. Cooper, *Chem. Sci.* **2020**, *11*, 543-550.
[56] a) S. Troppmann, B. König, *Chem.--Eur. J.* **2014**, *20*, 14570-14574; b) A. Wagner, K. H. Ly, N. Heidary, I. Szabó, T. Földes, K. I. Assaf, S. J. Barrow, K. Sokołowski, M. Al-Hada, N. Kornienko, M. F. Kuehnel, E. Rosta, I. Zebger, W. M. Nau, O. A. Scherman, E. Reisner, *ACS Catal.* **2020**, *10*, 751-761.
[57] Z. Xie, Y. Xu, J. Zheng, J. O. Lindner, X. Wen, N. Jiang, Z. Hu, L. Liu, F. Huang, F. Würthner, *Angew. Chem. Int. Ed.* **2020**, 10.1002/anie.202001231.
[58] M. Bajada, S. Roy, J. Warnan, K. Abdiaziz, A. Wagner, M. Roessler, E. Reisner, *Angew. Chem. Int. Ed.* **2020**, 10.1002/anie.202002680.
[59] P. Gai, W. Yu, H. Zhao, R. Qi, F. Li, L. Liu, F. Lv, S. Wang, *Angew. Chem. Int. Ed.* **2020**, *59*, 7224-7229.

REVIEW

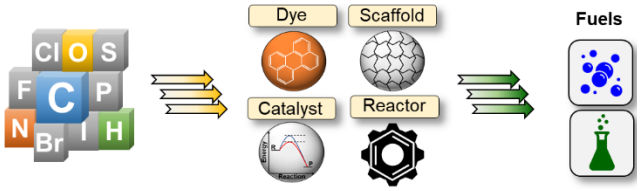

Julien Warnan, Erwin Reisner**

Page No. – Page No.

Synthetic Organic Design for Solar Fuel Systems

Organic and hybrid systems have emerged to challenge the classical inorganic structures through their enormous chemical diversity and modularity. Here, we discuss recent advances in the design of synthetic architectures and promising strategies toward (solar) fuel synthesis, highlighting progress on materials from dyes and catalysts to polymers and covalent organic frameworks.